

Development of a protocol for the imaging and diameter analysis of the common femoral vein in a tiltable MRI

BSc Thesis

L.J.C. Cordes

Committee Chair:
dr. ir. W.M. Brink

Daily Supervisor:
dr. ir. F.F.J. Simonis

External member:
dr. M.L. Groot Koerkamp

Biomedical Engineering
Faculty S&T

**UNIVERSITY
OF TWENTE.**

April 16, 2025

Abstract

Diameter measurements of (the iliofemoral) veins are sensitive to cross-sectional crush [1] and body position [2]. The diameter of a vein is of importance for the placement of venous stents in the treatment of iliofemoral Deep Vein Thrombosis (DVT). This research therefore investigated the development of an image acquisition protocol in a tiltable MRI to image the left common femoral vein (LCFV) in upright, supine, and hip flexion positions and a method for subsequent diameter analysis of the LCFV in these positions.

Multiple Magnetic Resonance Imaging (MRI) sequences were experimented with, with the sequences with the best initial results further optimized by variation of MRI parameters. For diameter analysis, the Maximum-Inscribed-Sphere (MIS) and Circular-Equivalent (CE) diameter offered by '3D Slicer' could be used.

The resulting image acquisition protocol comprises a T2 Fast Spin Echo (FSE) sequence for a good overview of pelvic anatomy and a Time-Of-Flight (TOF) sequence for the subsequent analysis of the diameter of the LCFV.

When comparing the LCFV in upright and supine positions, the acquired MRI images show that the LCFV has become twice as large. The CE diameter (upright) has increased to a range of approximately 9.2 - 15.2 mm and the MIS diameter to a range of approximately 7.6 - 12.0 mm compared to a range of 3.0 - 10.8 mm (CE, supine) and 2.5 - 8.8 mm (MIS, supine).

When comparing the LCFV in hip-flexion and supine positions, the acquired MRI images show that the LCFV has become 1,5 times larger. The CE diameter has grown to a range of approximately 7.5 - 13.2 mm (hip-flexion) and the MIS diameter to a range of 5.8 - 9.5 mm compared to the above mentioned ranges for the supine position.

The image quality from the upright scan implicated the diameter measurements in '3D Slicer' as the threshold value could not be set such that only the vein would be selected. It is suggested to investigate a way to reduce motion from the participant in upright position. Furthermore, flow-related ghosting artefacts presented with the TOF sequence and may also affect the diameter measurements. The Circular-Equivalent (CE) diameter is recommended for diameter measurement with the goal of stent placement.

Table of contents

1	Introduction	3
1.1	Research question and hypothesis	6
2	Method	6
2.1	Participants	6
2.2	Development process MRI image acquisition protocol	6
2.2.1	MRI system	6
2.2.2	Positioning	7
2.2.3	MRI sequence & parameter testing	7
2.3	Diameter measurements	7
2.4	Body position diameter comparisons	8
3	Results	8
3.1	MRI image acquisition protocol	8
3.1.1	T2 FSE sequence	8
3.1.2	Time-of-Flight sequence	10
3.2	Method for diameter measurement	12
3.2.1	Validity of the measures	12
3.3	Diameter dependency on body position	13
3.3.1	Supine versus upright body position	13
3.3.2	Supine versus hip-flexion body position	17
4	Discussion	20
4.1	Clinical implications	20
4.2	Study limitations	21
4.2.1	Image acquisition protocol	21
4.2.2	Method for diameter measurement	21
4.2.3	Diameter dependency on body position	22
5	Conclusion	22
A	Protocol MRI image acquisition	25
B	'3D Slicer' protocol for diameter measurements	28

List of Tables

1	An overview of the T2 FSE sequence parameters used for the MRI image acquisition.	9
2	An overview of the TOF sequence parameters used for the MRI image acquisition.	10
3	A comparison of the diameter values calculated by '3D Slicer' and manually acquired diameter values based on the MRI images.	13

1 Introduction

The May-Thurner syndrome, also known as Cockett syndrome or just iliac vein compression syndrome, is a medical condition where the left common iliac vein (LCIV) is compressed by the right iliac artery (RCIA) against the spinal column. See Figure 1 for an illustration of this. This syndrome is reported to affect 22% of the population [3]. Of the mentioned 22% of the population with May-Thurner syndrome, many people are asymptomatic [4]. Though May-Thurner is known to be a risk factor for left-sided iliofemoral Deep Vein Thrombosis (DVT) [3].

Notably, thrombus in the iliofemoral veins is considered the severest form of DVT, and DVT in itself is an important cause of short-term mortality and long-term impaired quality of life [6]. The most frequent subsequent complication occurring after iliofemoral DVT is known as post-thrombotic syndrome (PTS) [7]. With PTS, patients are not in lethal danger, but this condition could also potentially have a negative impact on the patients' quality of life, comparable to other chronic conditions such as heart failure or diabetes mellitus [8].

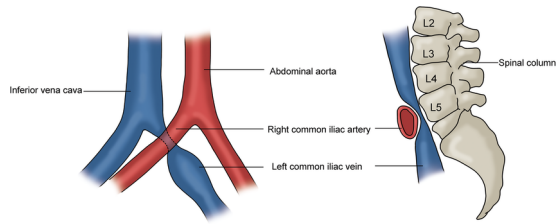


Figure 1: An illustration of the anatomy characteristic of May-Thurner syndrome: LCIV compression by the RCIA against the spinal column. Left, a coronal view and on the right a sagittal view [5].

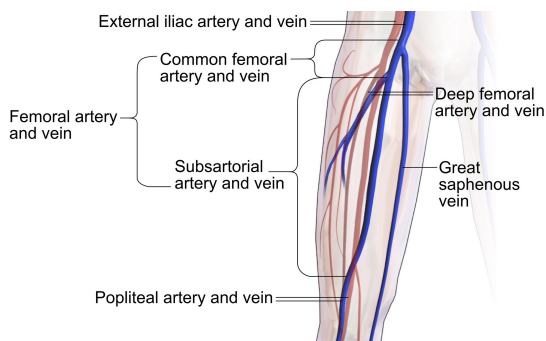


Figure 2: The anatomy of the iliofemoral artery and vein [9].

For the treatment of patients with PTS after having previously been diagnosed with iliofemoral DVT, endovenous stenting has become a preferred method [11], [12]. An example of such a stent is the 'Abre venous self-expanding stent system' by Medtronic or 'Sinus Venous' by Optimed [12]. Figure 3 shows a few of these venous stents. With the application of this treatment, it is very important to choose the appropriate stent diameter to minimize the risk of subsequent complications. Either undersizing or oversizing stents will likely lead to stent failure. Given that the iliofemoral veins have large diameters, the use of small diameter stents will compromise flow, leading to stenosis and occlusion, while oversizing a stent also has the potential to cause stenosis and occlusion, though distally in the vein. Another complication



Figure 3: Venous stents that are available on the European market [10].

that could occur with incorrect stent diameter selection is stent migration [13]. Stent migration is quite a rare complication but may be underreported [14].

To choose the appropriate diameter, a size of two mm greater than the measured reference vessel diameter of the iliofemoral vein is used to achieve good wall apposition of the stent [15]. In clinical practice, this reference vessel diameter is measured (on a non-diseased segment of the vein) using X-ray based angiography [16] or intravenous ultrasound (IVUS) using the cross-sectional area, considering the cross-section as a circle [16] [17]. See Figure 4 for an example of angiography.

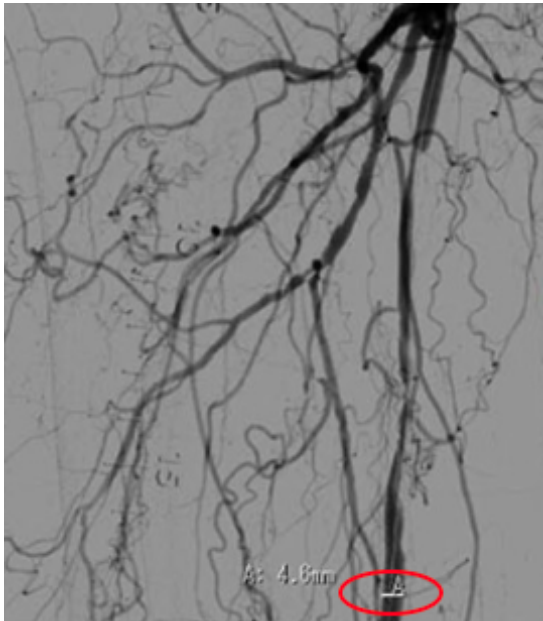


Figure 4: A reference vessel diameter determination using angiography. The measure within the red ellipse represents a diameter measurement on a healthy segment of the vein [16].

To determine whether a patient's symptoms are caused by May-Thurner Syndrome (MTS) and consequently treat the syndrome to prevent complications or prevent complications from recurring [19], a physical examination is insufficient [20]. Therefore, an imaging modality is needed for an accurate diagnosis. While there are multiple non-invasive imaging modalities that can be used for the diagnosis of May-Thurner syndrome, research has shown that MRI is the best modality for the diagnosis of this syndrome since it can rule out the presence of pelvic masses and iliofemoral DVT [21] while also being able to show the anatomy characteristic of May-Thurner syndrome [22]. Figure 5 shows how MTS can be diagnosed using MR venography.

Though ultrasound and CT are both more cost-efficient imaging modalities, both have significant disadvantages. Namely, direct ultrasound examination of the pelvic vessels has proven to be technically difficult [4] [22]. As a result, the accuracy of duplex ultrasound is reduced when visualizing pelvic



Figure 5: The May-Thurner anatomy characteristic by non-invasive MR venography: the left common iliac vein has a compression abnormality at Cockett's point (the crossing point of the right common iliac artery and left common iliac vein). See the red ellipse for the location of the compression abnormality [18].

and abdominal veins [23]. While with a CT scan, the diagnosis of chronic iliac vein pathosis is not possible through direct imaging, only by inference [22].

Previous research has shown the biomechanical structure of the pelvic region impacts the iliofemoral veins. It was observed that the superior ramus of the pubic bone compresses the CFV during hip extension, whilst this is not the case during hip flexion [1]. Figure 6 shows how the CFV runs with respect to the pelvis, and Figure 7 shows how the course of the CFV is changed with increased hip-flexion angle. This is interesting because the diameter of a vein is very sensitive to cross-sectional crush [1] and can take on different sizes depending on the position of the body. For example, the diameter of the common femoral vein has been shown to increase in an upright body position [2] [24]. Thus, body position has an impact on the diameter measurements of the common femoral vein. Taking this into account together with the notion that the diameter is a clinically critical anatomic parameter when assessing stent size [2], this research will investigate whether the diameter of the common femoral vein is subject to change when the hip is flexed and when the body is placed in an upright position. This will specifically comprise the left common femoral vein, as iliofemoral DVT most commonly occurs on the left side [6]. Furthermore, as there is yet no image acquisition protocol available for the imaging of the left common femoral vein (LCFV) on the tiltable MRI system, this study will comprise the development of such an image acquisition protocol. Lastly, a method for subsequent diameter measurements based on the acquired MRI images will be investigated.

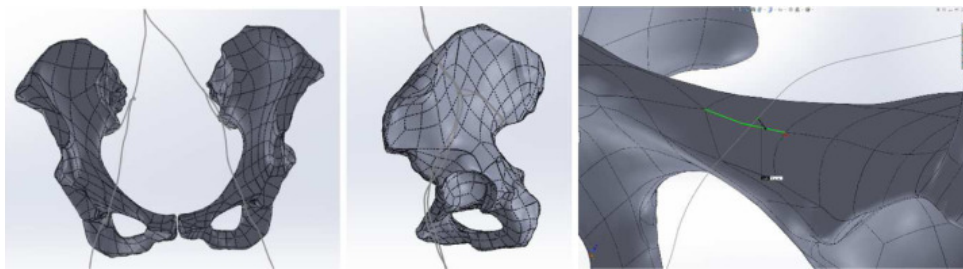


Figure 6: An overview of the iliofemoral vein centreline with respect to the bony structures of the pelvis. Of this section, the common femoral vein (CFV) centreline passes superiorly to the superior ramus of the pubic bone [1].

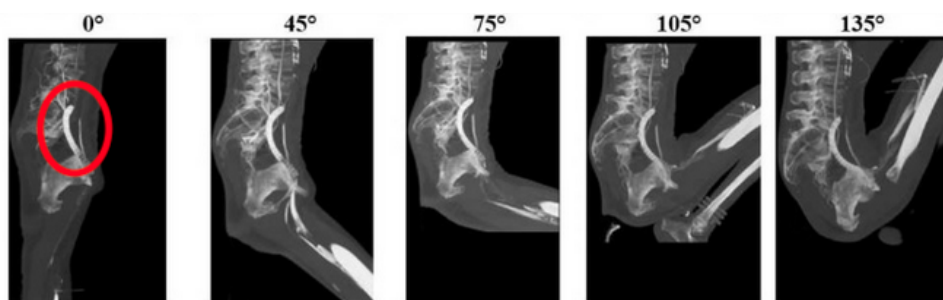


Figure 7: The course of the common femoral vein (stented) in one cadaver, as the hip flexion angle is increased. The stented common femoral vein (encircled by the red ellipse) becomes less compressed as a hip flexion angle is applied [1].

1.1 Research question and hypothesis

What is the influence of an upright body position and hip flexion angle on the diameter of the left common femoral vein (LCFV) in comparison with a supine body position, using a tiltable MRI for image acquisition?

To answer this question, the following sub-questions need to be answered:

- How can the LCFV segment be imaged with the tiltable MRI in a supine, upright and hip-flexed position?
- What method can be used for the purpose of diameter measurements based on the acquired MRI images?
- What is the effect of body position on the diameter of the LCFV?

It is hypothesized that an upright body position will cause an increase of about 20% in the diameter of the LCFV when comparing it with the diameter of the LCFV in a supine body position [2]. In addition to that, it is also expected that hip flexion will cause an increase in the diameter of the LCFV when comparing it with the diameter of the LCFV in hip extension (supine body position) [1].

2 Method

First, the method for the development of an image acquisition protocol for the imaging of the LCFV will be discussed. Secondly, it will be discussed how a method for diameter measurements based on the acquired MRI images can be chosen. Finally, a method for the comparison of diameter measurements in different body positions will be introduced.

2.1 Participants

During this study, four healthy participants, all of age in a range of 20-25 years and with a slim posture, were scanned. Of the participants, two were male and two were female.

Three of these participants were used for the sole purpose of MRI image acquisition protocol development. The data of the fourth participant were used for the results of the diameter measurement method and the comparison between body positions.

2.2 Development process MRI image acquisition protocol

This section will discuss the methods that were used for the purpose of developing an MRI image acquisition protocol for the imaging of the LCFV.

2.2.1 MRI system

The participants underwent an MRI examination with a 0,25 T tiltable MRI (G-Scan Brio by Esaote) using the 'Lumbar Spine 4-channels (medium size)' coil. This system allows for variation of the scanning position of the participant, something that is impossible with a conventional non-tiltable MRI system. In this study, the MRI system will be used at a tilt angle of 0° and 81°. Specifically, the table of the MRI system is tilted and as such the body of the participant as well.

2.2.2 Positioning

The MRI system was first tilted to an angle of 81° such that the participant could be scanned in an upright position. It is best to tilt the participant to a slightly lower angle than 90° so that the participant is able to lean somewhat backward and, with that, reduce discomfort. To reduce the chance of fainting of the participant [25], the imaging started with upright scanning.

The second part of the MRI examination was performed while the participant was in a supine position. The hips of the participant were fully extended in this position.

Finally, the participant was positioned such that the participant flexed the hip joint at an angle of about 35° . To make this position comfortable for the participant, a cushion was placed under the lower extremities of the participant. This also ensured the hip flexion angle of the participant remained fixed during the entire scanning procedure.



Figure 8: A participant placed in the MRI system in upright (A), supine (B) and hip-flexion (C) position.

2.2.3 MRI sequence & parameter testing

For the development of an appropriate image acquisition protocol on the tiltable MRI, the goal was to produce images of the LCFV with sufficient image quality for further analysis on the diameter of the LCFV. For this, first, the appropriate scanning region for the imaging of this vein needed to be determined. The acquired images from this scanning region required a well-distinguishable signal from the LCFV in terms of contrast, and its shape should be clearly distinguishable from other anatomy in the pelvic region of the body.

To achieve this, first, multiple 2D and 3D sequences were experimented with in the tiltable MRI. If the resulting images of such a sequence were not deemed initially sufficient according to the criteria on image quality described above, these sequences were no longer regarded for further optimisation. The sequences with the best initial results were further optimized by experimenting with the variation of multiple MRI parameters such as the slice thickness and the in-plane phase encoding direction.

2.3 Diameter measurements

For the diameter measurements, it is a requirement that these should be perpendicular to the centerline of the vein. The '3D Slicer' software offers a way of extracting this centerline. Therefore, the diameter measurement methods 'Maximum-Inscribed-Sphere (MIS) diameter' and 'Circular-Equivalent (CE) diameter' from '3D Slicer' were investigated. The MIS diameter

values take on the maximum diameter an inscribed sphere, with the centerline of the vein as the midpoint, can take on at each point along the centerline of the vein segment. The CE diameter values are determined by first assessing the cross-sectional area perpendicular to the centerline of the vein at that point on the centerline. Then, by calculating the diameter of a circle with an equivalent cross-sectional area, a value for the CE diameter can be obtained. See Figure 9 for a graphical representation of this.

Furthermore, as the diameter measurements should be able to give a true picture of reality, a comparison between manual measurements on the MRI images and the values from '3D Slicer' will be made.

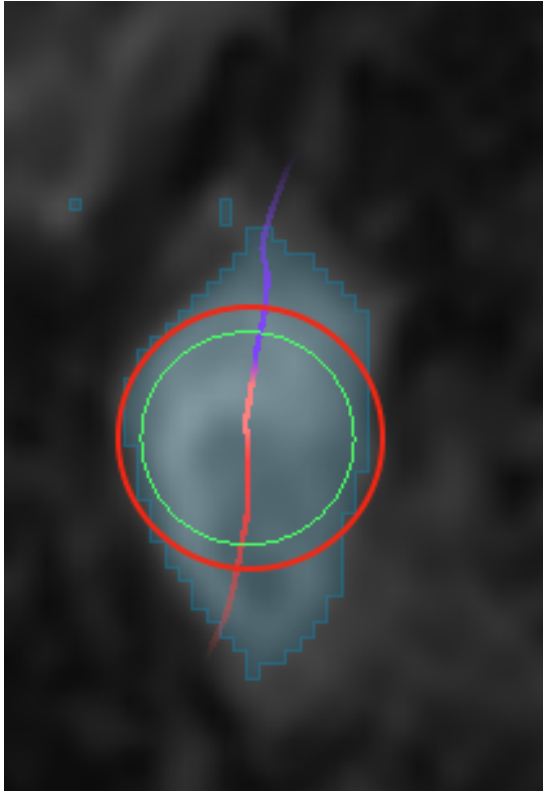


Figure 9: The green circle represents the cross-section of the maximum inscribed sphere (8,9 mm), while the red circle represents the circular-equivalent diameter (10,6 mm) based on the cross-section area of the vein model perpendicular to the centerline. The red-purple line in this Figure represents the centerline running through all scan slices, extracted by '3D Slicer'.

2.4 Body position diameter comparisons

Using the results from the MRI image acquisition protocol development and the investigation into a method for diameter measurements on the LCFV, comparisons will be made between a supine and upright body position and a supine and hip-flexion body position.

3 Results

3.1 MRI image acquisition protocol

This section will discuss the results from the development process of the image acquisition protocol.

3.1.1 T2 FSE sequence

This MRI sequence, with a duration of around three minutes, produced good images of the overall anatomy of the pelvic region. A disadvantage of the images of this sequence is that they show both the artery and the vein. As these lie next to each other (see Figure 2) and both show on the images with dark signal (black blood), it cannot be identified which of the two shapes

represents the common femoral artery and which the common femoral vein. So, with the T2 FSE sequence, no diameter can be obtained solely of the common femoral vein. Nonetheless, it provided a useful overview of the anatomy for the planning of the next MRI sequence in the image acquisition protocol. Figure 10A shows an image produced by the T2 FSE sequence in this study. Figure 10B shows how the scanning region was chosen such as to get an overview of the anatomy in the pelvic region.

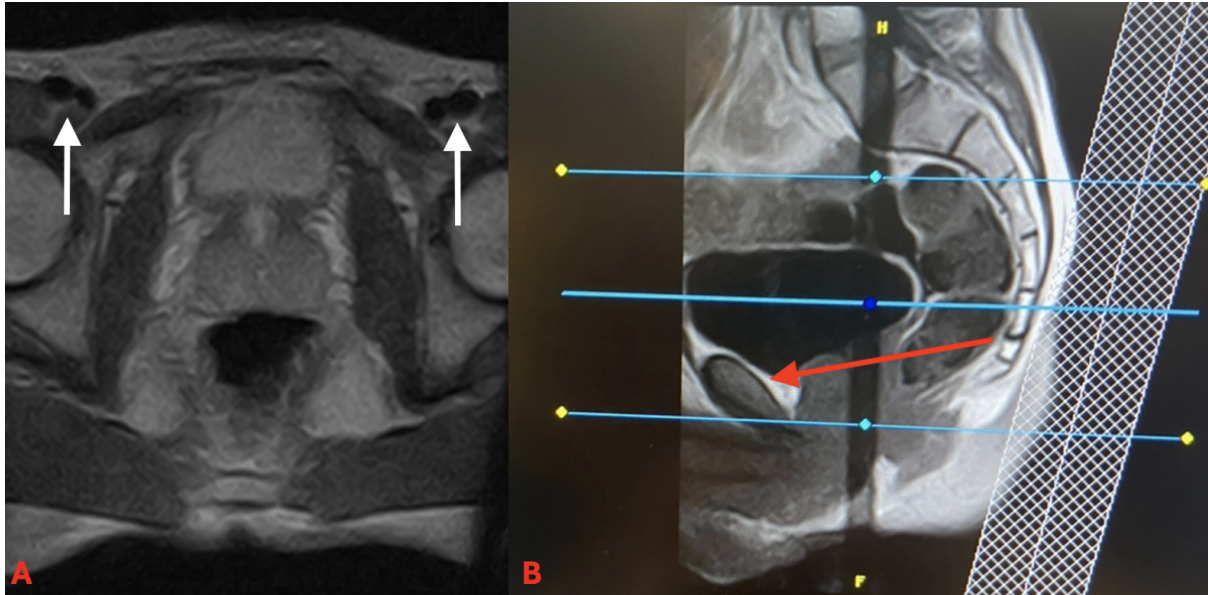


Figure 10: A) shows a resulting image from the T2 FSE sequence. The white arrows point to the neighbouring common femoral arteries and veins showing low signal intensity. B) shows the selection of the scanning region in a sagittal view, wherein the blue lines represent the middle and upper and lower boundaries of the scanning region. The red arrow points to the pubic symphysis, a useful anatomic landmark for the placement of the lower boundary.

Parameters T2 FSE sequence

For the T2 FSE sequence, the sequence parameters were set to the following values:

Table 1: An overview of the T2 FSE sequence parameters used for the MRI image acquisition.

Parameters	Value
Repetition time (TR)	7270 ms
Echo time (TE)	25 ms
Flip angle (FA)	90°
Nr. of voxels	512x512
Voxel size	0.55 mm x 0.55 mm x 5.0 mm
Slice thickness	5 mm
Spacing between slices	5 mm
Number of slices	23

3.1.2 Time-of-Flight sequence

The MRI imaging sequence used for the subsequent measurements was a 2D high-resolution Time-Of-Flight sequence (TOF) with the in-plane phase-encoding direction set to 'Column', from anterior to posterior (top to bottom in the image). This sequence was performed in the upright, hip-flexed, and supine body positions, where each scan took about eight minutes. The TOF sequence is a non-contrast MRI sequence producing images with bright blood [26]. See the example in Figure 11.

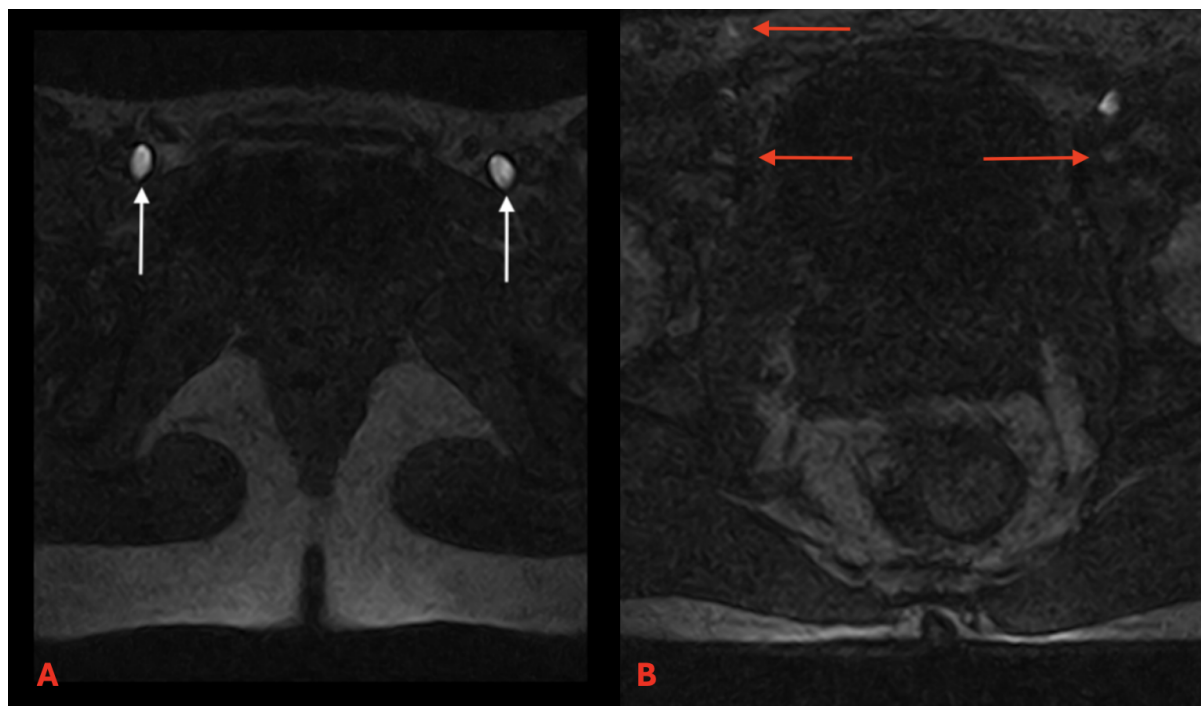


Figure 11: A) shows an image produced acquired in this study using the Time-Of-Flight (TOF) sequence with the Esaote tilttable 0,25 T MRI. The arrows point to the common femoral veins (CFV) showing high signal intensity (bright blood). B) shows another image acquired in this study using the TOF sequence. Unfortunately, the images may show flow-related ghosting artefacts (see red arrows) in the in-plane phase encoding direction, that is set from anterior to posterior direction (top to bottom in the image). [27] [28].

Parameters TOF sequence

For the TOF sequence, the sequence parameters were set to the following values:

Table 2: An overview of the TOF sequence parameters used for the MRI image acquisition.

Parameters	Value
Repetition time (TR)	45 ms
Echo time (TE)	10 ms
Flip angle (FA)	90°
Nr. of voxels	512x512
Voxel size	0.55 mm x 0.55 mm x 5.0 mm
Slice thickness	5 mm
Spacing between slices	N/A
Number of slices	17
In-plane phase encoding direction	Column

Settings scanning region

For the selection of the scanning region and the placement of the saturation block, the sagittal view image produced by a T2 Fast-Spin-Echo sequence (T2 FSE) was used (see section 3.1.1).

As the main interest lies in the common femoral vein segment running over the superior ramus of the pubic bone and not in the segment along the pubic symphysis or inferior to this structure, the scanning region was chosen as such. Furthermore, a saturation block was placed above the scanning region such that no signal from the common femoral arteries was visible. See Figure 12.

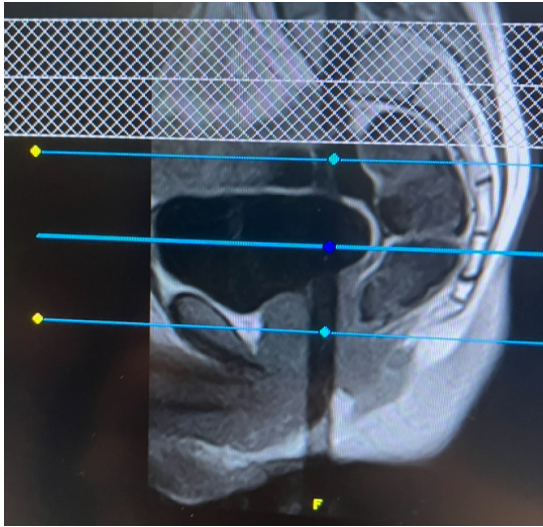


Figure 12: An overview of the selection of the scanning region and the placement of the saturation block in a sagittal view, wherein the blue lines represent the upper boundary, middle and lower boundary of the scanning region and the sloped lines the saturation block. The red arrow points to the pubic symphysis.

An overview of all the steps needed in the MRI examination of this study can be found in Appendix A.

3.2 Method for diameter measurement

A three-dimensional model was created from the MRI scan images acquired with the TOF sequence (section 3.1.2). Figure 13A shows how the model will initially look without any refining done. It shows a staircasing artifact, a limitation to the lengthwise accuracy of the model. With surface smoothing applied in '3D Slicer', the model will look like Figure 13B.

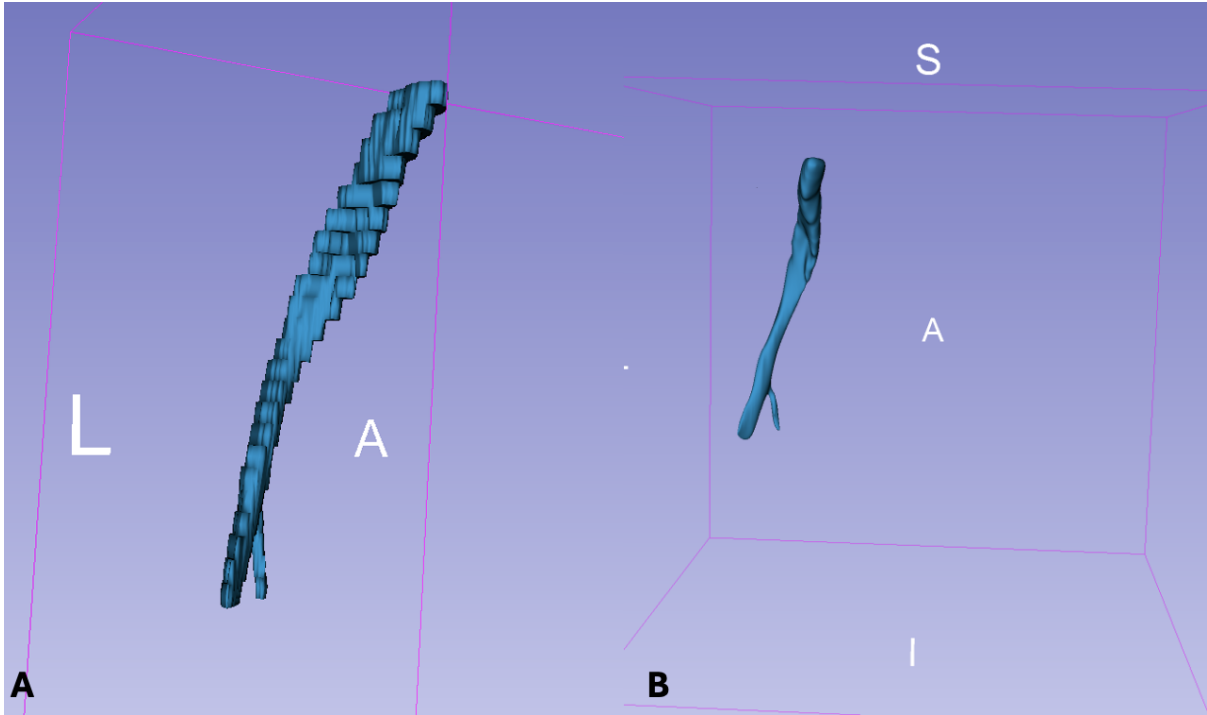


Figure 13: A) shows a three-dimensional model of the vein segment without the surface smoothing applied in '3D Slicer'. It shows how the 'building blocks' from the separate slices are stacked together to create the model. B) shows a three-dimensional model of the vein segment with the surface smoothing applied in '3D Slicer'. While the features of the segment are retained, the staircasing artifact is no longer visible.

As was mentioned in section 2.3, diameter analysis can be done either with the MIS diameter or the CE diameter. A notable difference between the MIS and CE diameter is the overall higher value of the CE diameter compared to the MIS diameter (see also Figures 18 and 22). This can be attributed to the non-circular shapes the vein takes on. For example, for ellipsoid shapes, the inscribed sphere (which takes the centerline as the midpoint of the sphere) will be smaller than the CE diameter (which is based on the cross-sectional area of the whole shape). See Figure 9.

3.2.1 Validity of the measures

To determine whether the diameter data from '3D Slicer' is realistic, both the MIS diameter and CE diameter are compared with measurements on the MRI images, taking the image corresponding to the point in the model where the diameter was calculated. For this purpose, the minimum MIS diameter and the corresponding CE diameter at that point in the model as given by '3D Slicer' can be found below together with the corresponding value from the manual measurement done on the MRI images.

Table 3: A comparison of the diameter values calculated by '3D Slicer' and manually acquired diameter values based on the MRI images.

MIS diameter [mm]		CE diameter [mm]	
3D Slicer	Manual	3D Slicer	Manual
3.32	3.77	6.00	7.39

From table 3, it can be acknowledged that the manually determined CE diameter tends to be higher than the CE diameter value determined by '3D Slicer'. The manually determined MIS diameter is quite close to the value determined by '3D Slicer'. With the manually determined values, it needs to be taken into account that these were not taken perpendicular to the centerline of the vein as the imaging plane was not oriented perpendicular to the centerline axis, contrary to the values from '3D Slicer'. This may result in a different cross-section shape [29]. And of course, adding to that, the control measures are manual in nature, and thus, more susceptible to manual measurement errors. This could explain differences in the obtained values. The manual measurements are shown in Figure 14.

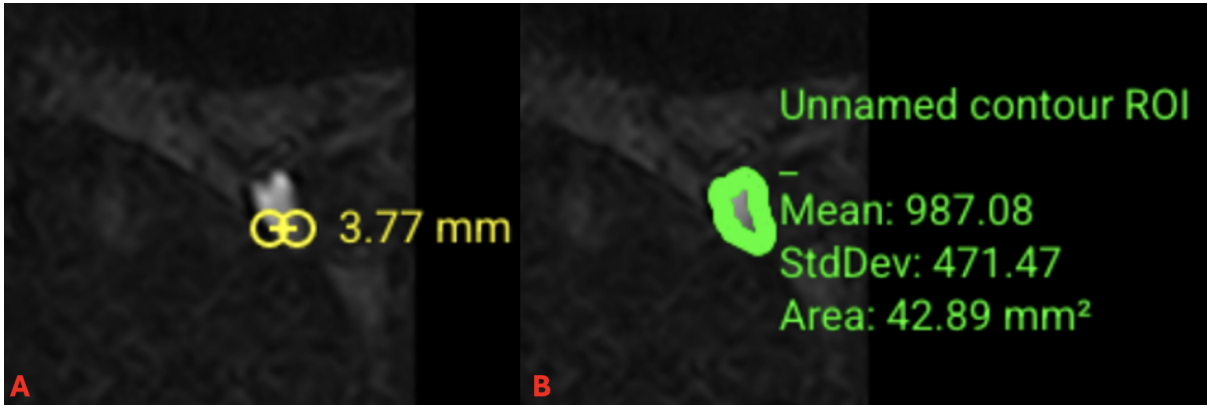


Figure 14: An overview of the manual measurements on the associated slice of the MRI scan for the minimum MIS diameter. A) shows the manual measurement done for a comparison with the MIS diameter. The length of the drawn line equals 3.77 mm. B) shows the manual measurement done for a comparison with the CE diameter. The area of the drawn contour equals approximately 43 mm².

A stepwise protocol for diameter measurement on the LCFV using '3D Slicer' can be found in Appendix B.

3.3 Diameter dependency on body position

This section will discuss the observations made from the MRI images, three-dimensional models, and the diameter measurements regarding the LCFV in different body positions.

3.3.1 Supine versus upright body position

First of all, the MRI images obtained from the developed image acquisition protocol showed the following findings as will be discussed based on Figures 15 and 16.

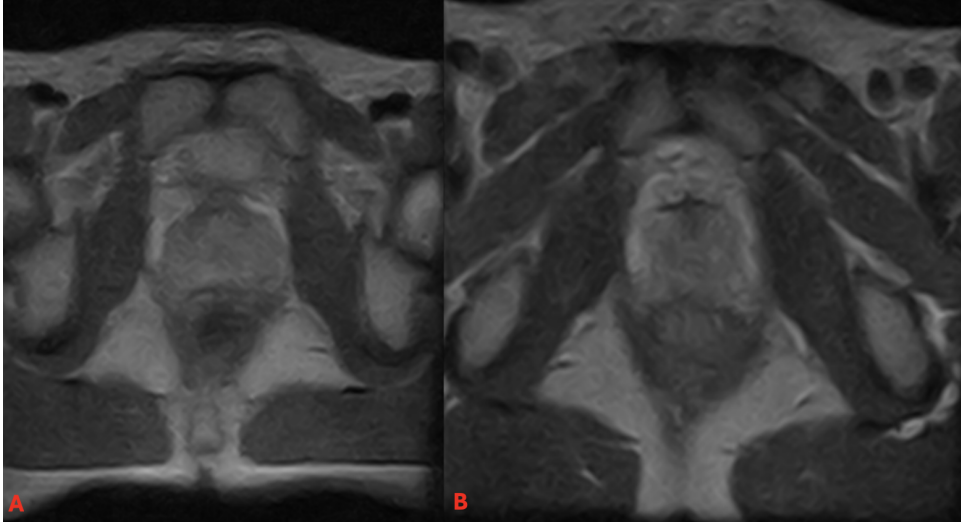


Figure 15: A comparison of the 20th slice of the T2 FSE scan in supine (A) and upright (B) position. The cross-section area of the vein has approximately become twice as large when the body is upright. Furthermore, the shape of the vein has become separable from the shape of the artery in the upright slice, unlike the supine slice.

So, from the T2 FSE scan (Figure 15) it can already be observed that the shape of the vein is subject to change. Namely, in the supine position, the vein shows a small circular shape, while, in the upright position, the vein takes on a larger ellipsoid shape. Moreover, the cross-sectional area of the vein shows an increase when comparing supine and upright positions. From manual measurement on the image, a doubling in size can be observed.

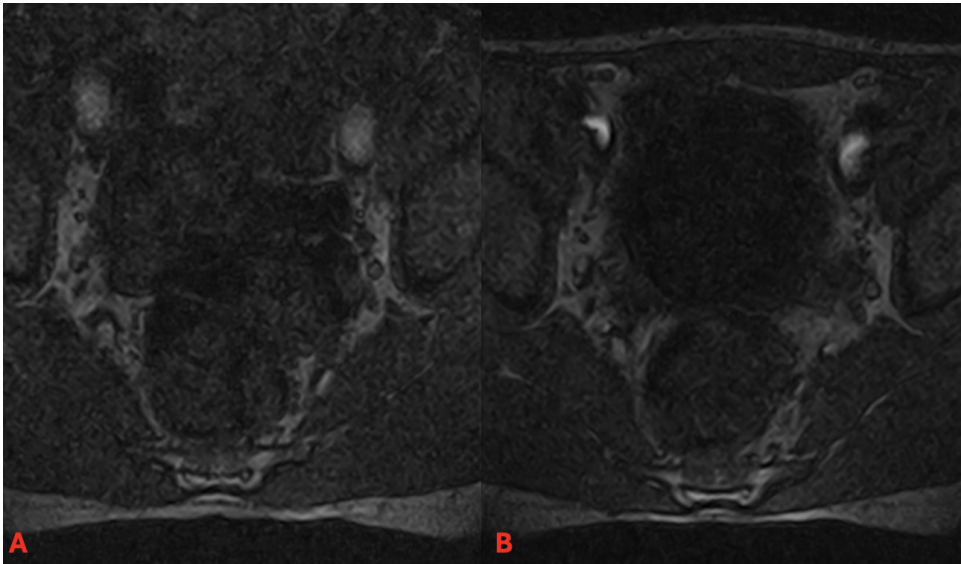


Figure 16: A comparison of the fourth slice of the TOF scan in supine (A) and upright (B) position. The signal from the vein is low in A), likely caused by motion artifacts coming from more movement of the participant in upright position. Next to that, it can be observed that the vein takes on different shapes in supine and upright position: A) shows an oval-like shape, B) a crescent-like shape.

In the images acquired from the TOF scan, again, it can be observed that the vein shows a change in shape when the body is upright compared to a supine position. Interestingly, the crescent-like shape in the supine position has changed into a large ellipsoid shape when standing

upright. The crescent-like shape can likely be attributed to compression by the superior pubic ramus, also see Figure 17 while the large ellipsoid shape in the upright position is caused by the increase of the hydrostatic pressure due to the effect of gravity [30]. In line with the T2 FSE, from the TOF sequence images, a cross-sectional area increase of a factor of two could also be determined through manual measurement.



Figure 17: The red ellipse encircles the section of the superior pubic ramus that likely causes the compression of the overlying tissue and CFV, leading to a crescent-like CFV.

The mentioned features in Figures 15 and 16 persist in the results of the diameter analysis below in Figure 18. Namely, as expected from the MRI images, both the CE and MIS diameters show higher values in the upright position compared to the supine position. The CE diameter (upright) has increased to a range of approximately 9.2 - 15.2 mm and the MIS diameter to a range of approximately 7.6 - 12.0 mm compared to a range of 3.0 - 10.8 mm (CE, supine) and 2.5 - 8.8 mm (MIS, supine). This is in line with the expectations, having the findings from Figure 16 in mind.

A second observation from Figure 18 is that the MIS diameter shows greater fluctuations in its value over the head to feet distance, especially in the supine position. This is likely due to the more varying shapes of the vein in this position as seen on the MRI images. The MIS diameter will show smaller values in the crescent-like segment compared to the rounder cross-sectional shapes in a different segment of the vein. The CE diameter is less sensitive to the type of shape the vein takes on due to its value depending on the overall cross-sectional area and does, therefore, not show similar fluctuations over the head to feet distance.

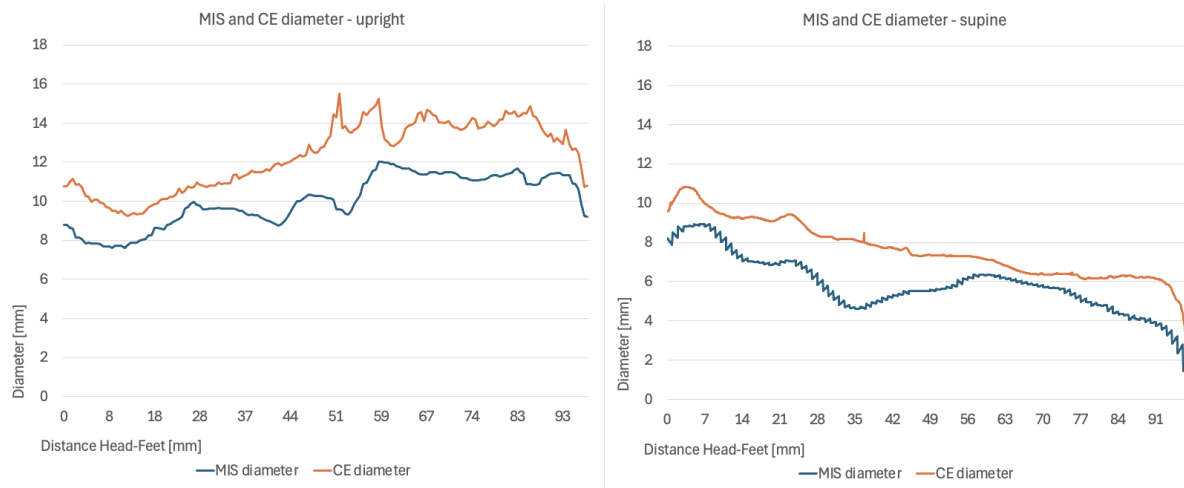


Figure 18: A comparison of the MIS and CE diameter of the three-dimensional models obtained from the upright and supine MRI scans.

Figure 19 shows the three-dimensional models on which the diameter measurements from Figure 18 are based. From the models, it can also be observed how the supine model has a more narrow shape at the inferior end and, thus, the diameter is smaller compared to the upright model. Furthermore, the mentioned crescent-like shapes in Figure 16 are visible in the supine model.

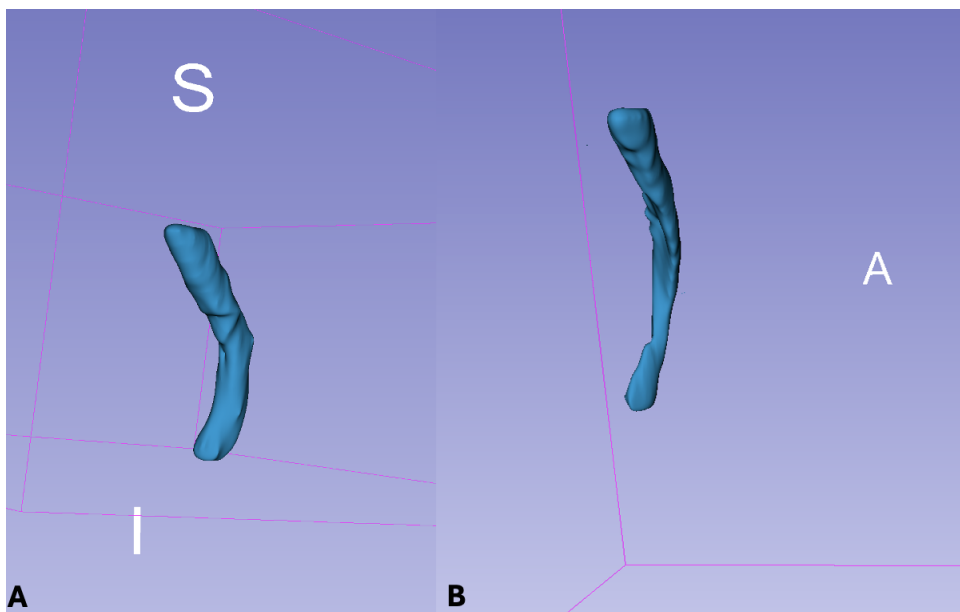


Figure 19: A) shows the upright three-dimensional model and B) shows the supine model.

As was discussed earlier, the SNR of the upright scan is low. An example of this is shown in Figure 20. The low SNR has an impact on the application of the threshold and subsequent correct segmentation. As can be seen, due to the low contrast of the CFV in the image, the threshold selects parts of the image that are irrelevant. This makes correct segmentation of the LCFV difficult, making many careful manual adjustments to the model needed.

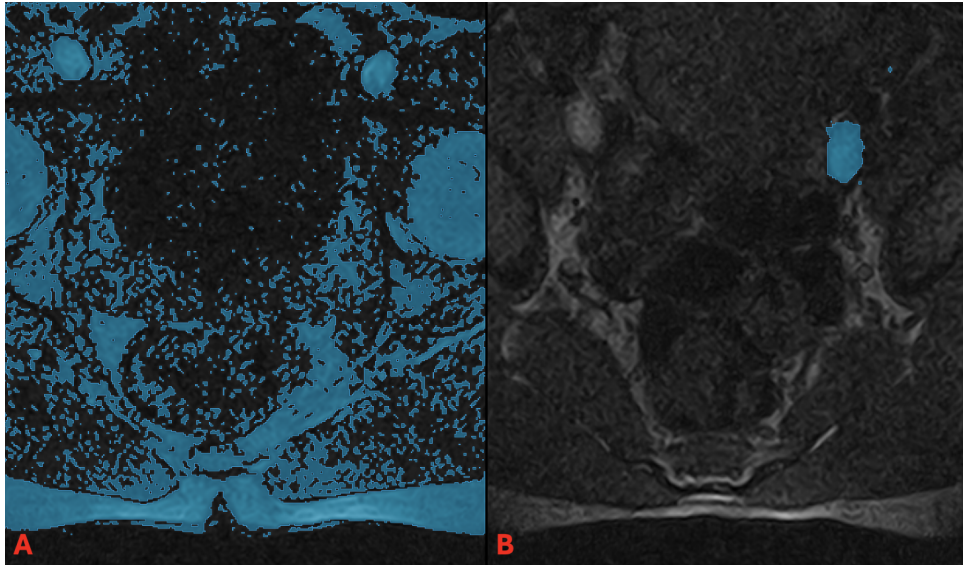


Figure 20: A shows how the threshold selects the CFV structures, but also many parts of the image that are irrelevant to the model. B shows the result after many careful manual adjustments to the model.

3.3.2 Supine versus hip-flexion body position

The MRI images obtained from the developed image acquisition protocol showed the following findings as will be discussed based on Figure 21.

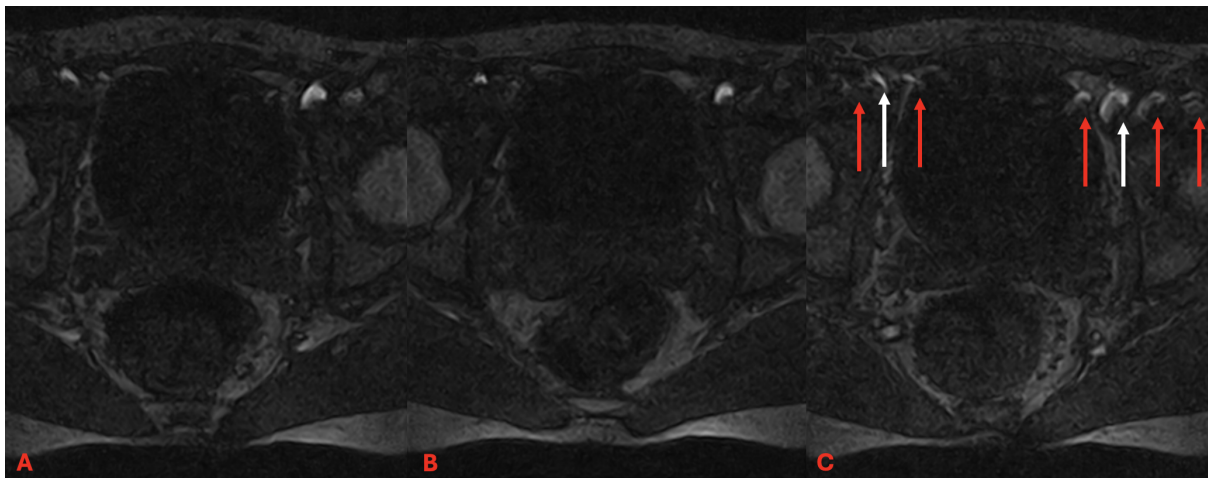


Figure 21: A comparison of the same slice of the TOF scan in hip-flexion (A) and supine (B) position. Both slices show a similar crescent-like shape of the vein. Though a difference can be observed in the vein's cross-section area; it has approximately become 1.5 times larger with hip-flexion at 35° . C) shows flow-related ghosting artefacts (red arrows) [27] [28] a TOF scan slice in hip-flexion position. The white arrows point to the shape of the original vein. These artefacts were not as visible in the supine scan, but showed visibly in multiple slices of the hip-flexion scan.

In Figure 21, there is a key difference in the cross-sectional area, namely that it has increased by a factor of 1.5 when comparing the hip-flexion position with the supine position. Furthermore, the hip-flexion scan shows substantially more flow-related ghosting artefacts in the phase-encode direction, whereas these are nearly non-existent in the supine scan. These occur whenever the position or signal intensity of imaged structures vary or move regularly, in this case due to

vascular flow. The intensity of these vascular ghosting artefacts increases with the amplitude of the periodic motion. For the spacing of the vascular ghosts, generally, they will be spaced more widely with increasing flow velocity [31]. So, a cause of the increased presence of the vascular ghosts in the hip-flexion scan could be that the flow velocity in the LCFV is more rapid compared to the flow velocity in a supine position.

In Figure 18 the results of the diameter measurements performed in the hip-flexion and supine position are presented.

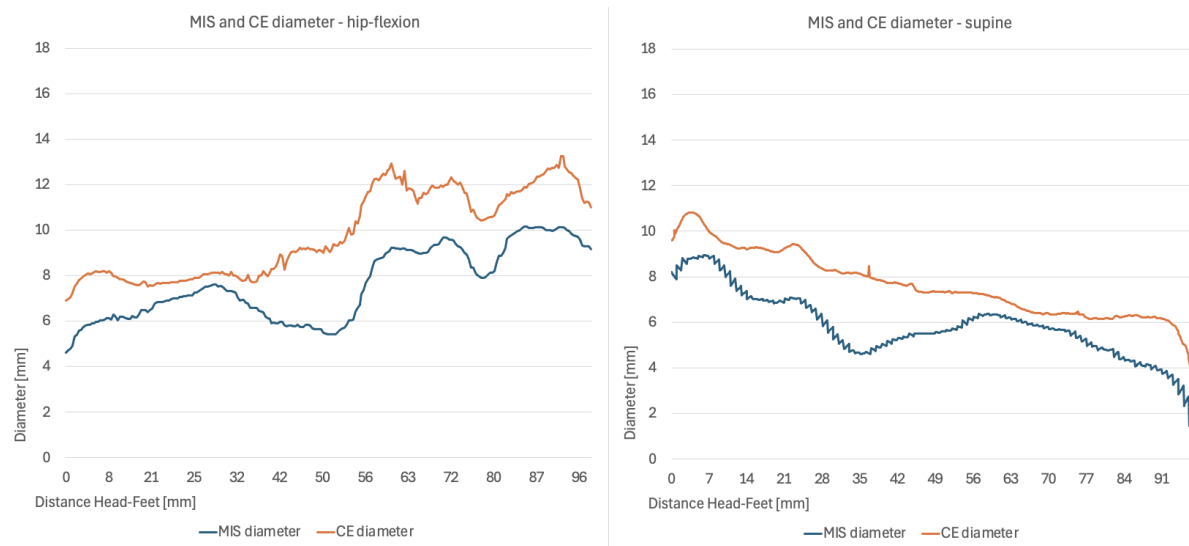


Figure 22: A comparison of the MIS and CE diameter of the three-dimensional models obtained from the hip-flexion and supine MRI scans.

Figure 22 shows the initial segment of the LCFV in hip-flexion has a smaller CE and MIS diameter when comparing it with the supine position. With increasing head to feet distance, the CE diameter increases. The MIS diameter also shows an increase, after an initial drop to approximately 5.8 mm. Overall, the CE diameter has grown to a range of approximately 7.5 - 13.2 mm (hip-flexion) and the MIS diameter to a range of 5.8 - 9.5 mm compared to a range of 3.0 - 10.8 mm (CE, supine) and 2.5 - 8.8 mm (MIS, supine).

The initial smaller value of the hip-flexion diameters does not seem to be correct based on the MRI images, as the MRI images show these values should be a factor of 1.5 times greater than the supine values. A cause of this underestimation could be attributed to incorrect segmentation of the hip-flexion model in the initial slices due to blurriness from the artifacts in the hip flexion MRI images. See Figure 23 for an example.

The initial drop of the MIS diameter is likely due to crescent-like shapes also being present in the MRI images taken in the hip-flexion position. Lastly, the greater range of values of the MIS and CE diameter values in the model when comparing with the supine model is in line with the findings shown in Figure 21.

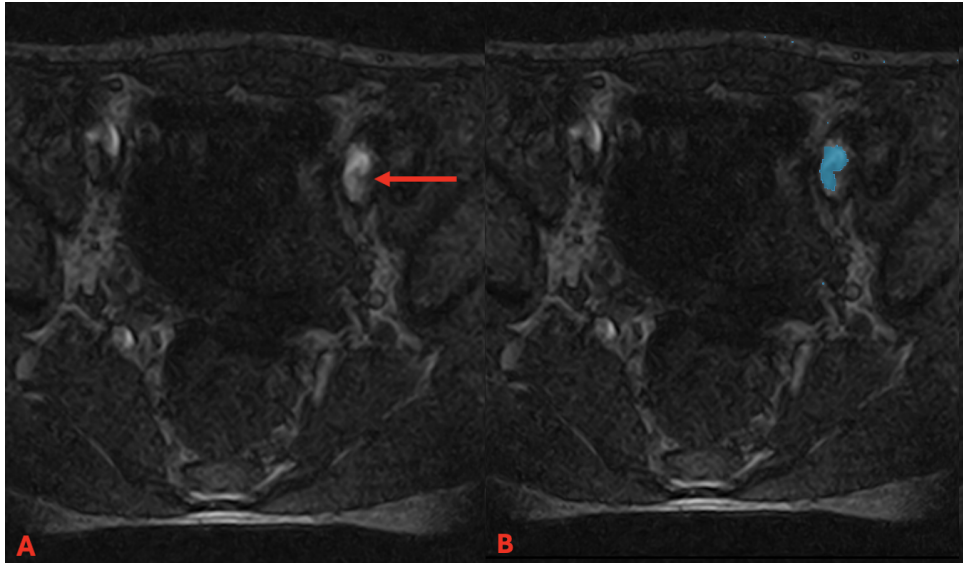


Figure 23: A) shows one of the first slices in the hip-flexion MRI scan and B) the corresponding slice with the threshold markups. When comparing A) and B), it can be observed that the threshold markup does not encompass the full shape of the LCFV, likely due to the blurring at the edge of the shape. Consequently, the diameter calculation shows lower values for this section.

Figure 24 shows the three-dimensional models on which the diameter measurements from Figure 18 are based. The models are quite similar to each other, as expected from the findings of the MRI images (Figure 21).

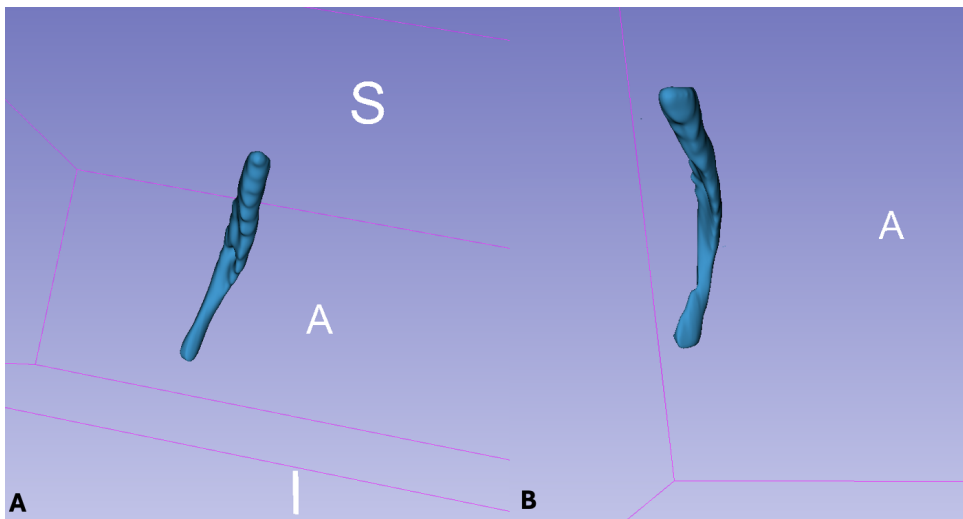


Figure 24: A) shows the hip-flexion model and B) shows the supine model.

4 Discussion

The development of an MRI image acquisition protocol for the imaging of the LCFV in the tiltable MRI proved to be successful. A T2 FSE sequence can be used to provide a good overview of the pelvic anatomy, which is useful to see what impact the surrounding anatomy has on the CFV. A TOF sequence can then be used for diameter analysis on the LCFV. For the diameter measurements, the MIS and CE diameter of '3D Slicer' can be used as they are both valid measures.

When comparing the results of the MRI image acquisition and the diameter measurements between the body positions, interesting observations could be made. First of all, it could indeed be observed that the diameter of the LCFV increases in an upright body position. The noted changes in vein shape and overall cross-section area obtained from comparisons of MRI images reflected well in the diameter measurements that were done subsequently. This is in line with previous research [2]. Though, the observed increases (maximum CE diameter increase of 40%, minimum CE diameter increase of nearly 200%) were greater than ascertained in the paper of Keiler et. al., 2018. As this paper used a different method for the diameter analysis, namely, determination of the mean diameter from cross measurements using duplex ultrasound as an imaging modality, this likely explains why there is a difference in the observed diameter increases.

Secondly, it could newly be ascertained that the diameter of the LCFV, unstented and in live participants, increases with hip-flexion. Though vein shape remained rather similar to the vein shape in a supine position, its cross-sectional area increased with a factor of 1.5. This was also visible in the diameter measurements, that showed an increase of the minimum CE diameter of around 20% and the maximum CE diameter by around 30%.

Lastly, as the study from Cheng et. al, 2020 pointed out, the CFV is compressed by the superior ramus of the pubic bone when the body is placed in a supine position. In this study, this phenomenon showed through crescent-like vein shapes in multiple slices of the T2 FSE and TOF supine scans. With increased hip-flexion angle, the LCFV becomes less compressed by the superior ramus as proven by Cheng et. al., 2020. This study newly showed that this effect also reflects in the diameter measurements.

4.1 Clinical implications

In clinical practice, as was previously mentioned, the reference vessel diameter (RVD) is measured either with angiography [16] or IVUS [16] [17]. In this study, both diameter measures offered by '3D Slicer' were used. Though the MIS diameter characterizes the shape of the vein more by showing smaller values in crescent-like and thin shapes, it is recommended to take the CE diameter for the assessment of the diameter of the vein, as it is able to determine the diameter of the vein more independently of its shape. In the paper of Iida et. al., 2021, a method similar to the '3D Slicer' CE diameter is employed using IVUS. It used the external elastic membrane cross-sectional area, considering the cross-section as a circle, for the determination of the value of the RVD. So, with the purpose of placing a correctly sized stent, it is recommended to use the CE diameter and not the MIS diameter.

As for the observed increases in the diameter of the LCFV in an upright and hip-flexion position and its implications on the determination of correct stent size, more research is needed to determine whether it is better to measure the RVD in either an upright or hip-flexion position instead of a supine position. Basing stent size on an RVD measured in either an upright or hip-flexion position will lead to the choosing of larger sized stents. How this impacts the clinical outcomes of venous interventions and, thus, whether it is the right choice, is yet unknown.

4.2 Study limitations

When reproducing this study with a greater sample size, it must be taken into account that not every participant may fit in the MRI system with the hips flexed at an angle of approximately 35°. Therefore, preferably, participants are selected that are of slim stature and do not have large knees as these may not fit within the magnet when the limbs are placed at the mentioned angle. As the CFV diameter is, among others, dependent on BMI [2], this limitation has the consequence that the selection of participants in this study will not represent the entire population.

4.2.1 Image acquisition protocol

Several limitations must be acknowledged regarding the image acquisition protocol.

At the moment, the total scan duration of this image acquisition protocol is rather long, with the T2 FSE sequence taking about three minutes and the TOF sequence around eight minutes. As it is very important for the resulting image quality that the participant is able to stand or lie still during scanning, participants of the study may experience discomfort. Especially when the participant is scanned in an upright position, scan duration is a limiting factor. During this study, it was shortly experimented with acquiring separate slices instead of as a pack. Separate slice acquisitions were finished twice as fast. A suggestion to achieve reduced scan duration is therefore to acquire all slices separately. For further analysis in '3D Slicer', the application of this method for image acquisition requires all acquired slices to be put in one folder.

Secondly, as discussed in section 3.3.1 the signal-to-noise ratio (SNR) from the upright MRI scan is low. This was also observed in the resulting upright MRI scans during the ongoing development of the image acquisition protocol. Poor image quality implicates the correct segmentation of the three-dimensional model based on the MRI images, as many careful manual adjustments are needed after applying a threshold (see Figure 20) possibly negatively affecting the veracity of the diameter analysis. Motion of the participant could be a cause of the poor image quality. Participants may experience more difficulty standing completely still than lying still during image acquisition. Future research is needed to investigate whether this is indeed the cause of the poor image quality in upright MRI scans. A suggestion is to experiment with more fixation of the participant in upright scanning with cushions, for example.

Finally, as discussed in section 3, the flow-related ghosting artifacts may present with the TOF sequence, especially in the hip-flexion scans, and could also impact the diameter analysis in the way that was discussed in section 3.3.2. A suggestion for a possible solution to the presence of vascular ghosts in the acquired MRI images is to investigate the use of flow compensation gradients [32].

4.2.2 Method for diameter measurement

A limitation regarding the method for diameter measurements is the longitudinal preciseness of the three-dimensional model of the LCFV. Lengthwise, the model's capability to match the actual vein is limited by the slice thickness (five mm in this study) used with image acquisition (see Figure 13A in section 3.2). If it is desired to further improve the model's veracity compared to the actual vein, a solution may be to reduce the slice thickness during image acquisition. However, consequently, the number of slices acquired must be increased to obtain a model of the same length. As a result of this, the MRI scan will take longer, which has its previously mentioned limitations. With the slice thickness set to, for example, three mm instead of five mm, the scan will likely take around 13 minutes instead of the previously eight minutes. Furthermore, a smaller slice thickness was experimented with to see what effect this would have on the image quality. This, though, caused a decrease in image quality, making further analysis with '3D

'Slicer' no longer possible with the acquired images. It is therefore suggested to stick with a slice thickness of five mm despite the limitation to the model.

4.2.3 Diameter dependency on body position

The small sample size ($n=1$) limits the generalizability of these results. A larger group of participants is needed to identify whether these findings persist in a larger group of participants and, as such, in the population. Since previous research [1] suggests not every participant shows the same pattern of the CFV being compressed by the pubis in the supine position; thus, the findings of this study for the hip flexion position may or may not differ from what is present in the population. The mentioned previously conducted study ([1]) used 36 limbs for its analysis. Therefore, specifically looking at the LCFV as was done in this study, an amount of around 30-45 participants is recommended for further research on potential trends in the diameter of the LCFV on hip flexion-extension in live participants.

5 Conclusion

In this study, a protocol for image acquisition and diameter analysis of the LCFV was developed with subsequent LCFV diameter evaluation in upright, supine, and hip-flexion positions. Image acquisition of the LCFV segment with the tiltable MRI is possible using a T2 FSE sequence (black blood) and a TOF sequence (bright blood). For diameter measurements, the MIS and CE diameter measures offered in '3D Slicer' are both valid methods. Though, for the diameter assessment of the vein with the purpose of placing a correctly sized stent, the CE diameter is recommended.

When comparing the diameter measurements of the LCFV in a supine and upright body position, the values of the diameter measurements of the LCFV are higher in an upright position. The maximum CE diameter has increased by 40% and the minimum CE diameter by nearly 200%. This is an even greater increase than was expected. For the diameter of the LCFV in hip-flexion, as was expected, the diameter values have increased. The maximum CE diameter has increased by about 30% and the minimum CE diameter by around 20%.

References

- [1] “The biomechanical impact of hip movement on iliofemoral venous anatomy and stenting for deep venous thrombosis,” *Journal of Vascular Surgery: Venous and Lymphatic Disorders*, vol. 8, no. 6, pp. 953–960, 2020, ISSN: 2213-333X. DOI: <https://doi.org/10.1016/j.jvsv.2020.01.022>.
- [2] J. Keiler, R. Seidel, and A. Wree, “The femoral vein diameter and its correlation with sex, age and body mass index—an anatomical parameter with clinical relevance,” *Phlebology*, vol. 34, no. 1, pp. 58–69, 2019.
- [3] S. Carr, K. Chan, J. Rosenberg, *et al.*, “Correlation of the diameter of the left common iliac vein with the risk of lower-extremity deep venous thrombosis,” *Journal of vascular and interventional radiology*, vol. 23, no. 11, pp. 1467–1472, 2012.
- [4] R. P. Liddell and N. S. Evans, “May-thurner syndrome,” *Vascular Medicine*, vol. 23, no. 5, pp. 493–496, 2018.
- [5] Y. Liu, H. Zheng, X. Wang, *et al.*, “Ultrasound characteristics of abdominal vascular compression syndromes,” *Frontiers in cardiovascular medicine*, vol. 10, p. 1282597, 2023.
- [6] N. Denny, S. Musale, H. Edlin, F. Serracino-Inglott, and J. Thachil, “Iliofemoral deep vein thrombosis and the problem of post-thrombotic syndrome,” *Acute Med*, vol. 17, no. 2, pp. 99–103, 2018.
- [7] M. Costa, G. Ferreira, D. Gomes, C. Oliveira, and N. Domingues, “May-thurner syndrome: The worst-case scenario,” *Cureus*, vol. 16, no. 3, 2024.
- [8] I. Makedonov, S. R. Kahn, and J.-P. Galanaud, “Prevention and management of the post-thrombotic syndrome,” *Journal of clinical medicine*, vol. 9, no. 4, p. 923, 2020.
- [9] C. Amarnath, H. Patel, A. Irodi, *et al.*, *Comprehensive Textbook of Clinical Radiology: Chest and Cardiovascular System, Volume 3 - EBook*. Elsevier Health Sciences, 2023, ISBN: 9788131263624. [Online]. Available: https://books.google.nl/books?id=_3i_EAAAQBAJ.
- [10] E. Avgerinos and H. Jalaie, “Progress in the management of early thrombus removal,” *Phlebology*, vol. 30, no. 3, pp. 118–124, 2023.
- [11] K. Breen, “Role of venous stenting for venous thromboembolism,” *Hematology 2014, the American Society of Hematology Education Program Book*, vol. 2020, no. 1, pp. 606–611, 2020.
- [12] “A clinical guide to deep venous stenting for chronic iliofemoral venous obstruction,” *Journal of Vascular Surgery: Venous and Lymphatic Disorders*, vol. 10, no. 1, 258–266.e1, 2022, ISSN: 2213-333X. DOI: <https://doi.org/10.1016/j.jvsv.2020.12.087>.
- [13] H. Kim *et al.*, “Cases of venous stent failure in lower extremities,” *Annals of Phlebology*, vol. 21, no. 2, pp. 90–94, 2023.
- [14] M. H. Sayed, M. Salem, K. R. Desai, G. J. O’Sullivan, and S. A. Black, “A review of the incidence, outcome, and management of venous stent migration,” *Journal of Vascular Surgery: Venous and Lymphatic Disorders*, vol. 10, no. 2, pp. 482–490, 2022.
- [15] “Three-year outcomes of the abre venous self-expanding stent system in patients with symptomatic iliofemoral venous outflow obstruction,” *Journal of Vascular and Interventional Radiology*, vol. 35, no. 5, 664–675.e5, 2024, ISSN: 1051-0443. DOI: <https://doi.org/10.1016/j.jvir.2024.01.030>.
- [16] O. Iida, M. Takahara, Y. Soga, *et al.*, “Vessel diameter evaluated by intravascular ultrasound versus angiography,” *Journal of Endovascular Therapy*, vol. 29, no. 3, pp. 343–349, 2022.

- [17] N. Labropoulos, M. Borge, K. Pierce, and P. J. Pappas, “Criteria for defining significant central vein stenosis with duplex ultrasound,” *Journal of Vascular surgery*, vol. 46, no. 1, pp. 101–107, 2007.
- [18] C. Simon, J. Alvarez Jr, G. J. Becker, B. T. Katzen, J. F. Benenati, and G. Zemel, “May-thurner syndrome in an adolescent: Persistence despite operative management,” *Journal of vascular surgery*, vol. 30, no. 5, pp. 950–953, 1999.
- [19] M.-G. Knuttinen, S. Naidu, R. Oklu, *et al.*, “May-thurner: Diagnosis and endovascular management,” *Cardiovascular diagnosis and therapy*, vol. 7, no. Suppl 3, S159, 2017.
- [20] M. M. Harbin and P. L. Lutsey, “May-thurner syndrome: History of understanding and need for defining population prevalence,” *Journal of Thrombosis and Haemostasis*, vol. 18, no. 3, pp. 534–542, 2020.
- [21] L. Lyhne, K. C. Houliind, J. Christensen, *et al.*, “Magnetic resonance imaging as a diagnostic tool for ilio-femoro-caval deep venous thrombosis,” *Journal of Imaging*, vol. 10, no. 3, p. 66, 2024.
- [22] L. M. Wolpert, O. Rahmani, B. Stein, J. J. Gallagher, and A. D. Drezner, “Magnetic resonance venography in the diagnosis and management of may-thurner syndrome,” *Vascular and endovascular surgery*, vol. 36, no. 1, pp. 51–57, 2002.
- [23] V. G. Helyar, Y. Gupta, L. Blakeway, G. Charles-Edwards, K. Katsanos, and N. Karunanithy, “Depiction of lower limb venous anatomy in patients undergoing interventional deep venous reconstruction—the role of balanced steady state free precession mri,” *The British Journal of Radiology*, vol. 91, no. 1082, p. 20170005, 2018.
- [24] J. K. van Zandwijk, J. A. Simmering, R. C. Schuurmann, *et al.*, “Position-and posture-dependent vascular imaging—a scoping review,” *European radiology*, vol. 34, no. 4, pp. 2334–2351, 2024.
- [25] B. B. Hansen, R. Bouert, H. Bliddal, *et al.*, “External pneumatic compression device prevents fainting in standing weight-bearing mri: A cohort study,” *Skeletal radiology*, vol. 42, pp. 1437–1442, 2013.
- [26] S.-E. Kim and D. Parker, “Time-of-flight angiography,” in Jan. 2012, pp. 39–50, ISBN: 978-1-4419-1685-3. DOI: 10.1007/978-1-4419-1686-0_2.
- [27] M. Zaitsev, J. Maclaren, and M. Herbst, “Motion artifacts in mri: A complex problem with many partial solutions,” *Journal of Magnetic Resonance Imaging*, vol. 42, no. 4, pp. 887–901, 2015.
- [28] L. Axel, “Blood flow effects in magnetic resonance imaging,” *American journal of roentgenology*, vol. 143, no. 6, pp. 1157–1166, 1984.
- [29] Y.-R. Gao and P. J. Drew, “Determination of vessel cross-sectional area by thresholding in radon space,” *Journal of Cerebral Blood Flow & Metabolism*, vol. 34, no. 7, pp. 1180–1187, 2014.
- [30] H. Hinghofer-Szalkay, “Gravity, the hydrostatic indifference concept and the cardiovascular system,” *European journal of applied physiology*, vol. 111, pp. 163–174, 2011.
- [31] M. L. Wood and R. M. Henkelman, “Mr image artifacts from periodic motion,” *Medical physics*, vol. 12, no. 2, pp. 143–151, 1985.
- [32] R. Hashemi, W. Bradley, and C. Lisanti, *MRI: The Basics* (The Basics Series). Lippincott Williams & Wilkins, 2010, ISBN: 9781608311156. [Online]. Available: <https://books.google.nl/books?id=v4LFgAHxNz4C>.

A Protocol MRI image acquisition

The full imaging protocol stepwise:

1. Create a project in the Esaote software. In this study, 'Esaote iliofemoral imaging';
2. Create a 'subject' folder for the yet-to-be-acquired data of the study participant. The name of this folder should be fully anonymized. Therefore, 'iliofemoral_pp0'. 'iliofemoral_pp1' etc. is recommended;
3. Fill out the subject details in the Esaote software. Select the 'Patient's Sex' as 'O', the 'Patient's Birth Date' as the date on which this protocol is executed on the subject, set the 'Patient's Size' to 0 and the 'Patient's Weight' also to 0;
4. Select the body part examined as 'LSPINE' and make sure the subject position is set to 'head on right';
5. Select the 'Receive Coil name' as '17';
6. Participant takes place in the MRI system;
7. The participant may lie down on their back (supine position) on the table of the MRI system with the head on the right;
8. If the participant is comfortable, attach the coil to the table and attach the cable to the MRI system;
9. Instruct the participant (if necessary) to move such that the groin of the participant is placed in the coil. The pubic bone of the participant should be in the centre of the coil;
10. Start the preview sequence on the touchscreen of the MRI system. Choose the sagittal view;
11. Check whether the pubic bone of the participant is in the centre of the image shown on the screen of the MRI system. The horizontal crosshair line should run slightly above the pubic symphysis (see Figure 25 for how the pubic symphysis looks like on the Scout);
12. Reposition the participant if necessary (and repeat steps 10 and 11) ;
13. Check whether the participant is in the middle of the coil by choosing the axial view from the preview. The vertical crosshair from the preview should be in the middle of the axial view.
14. Inform the participant of the importance of lying still throughout the examination, especially when the MRI system is making sounds. If the MRI system is silent, the participant can shortly move if the participant desires to do so. The full imaging protocol will take about an hour in total;
15. If the participant is ready, let the MRI system tilt to an angle of 81°;
16. Perform the Scout sequence. See Figure 25;

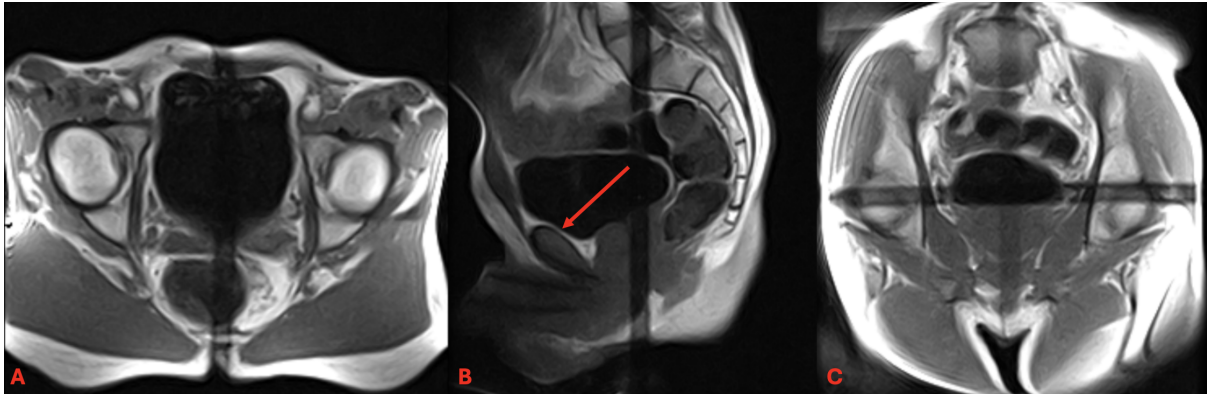


Figure 25: An overview of the images produced by the Scout (on Esaote tilttable 0,25 T MRI) with correct positioning of the participant. A) shows an axial view wherein the centre has been placed approximately at the femoral head and in the middle of the bottom of the participant. B) shows a sagittal view wherein the middle is placed slightly superior to the pubic symphysis (see red arrow). Finally, C) shows a coronal view where the bony structures of the pelvis can be seen on the lateral sides of the participant. The vertical middle is placed at the participant's crotch and the horizontal middle along the femoral head.

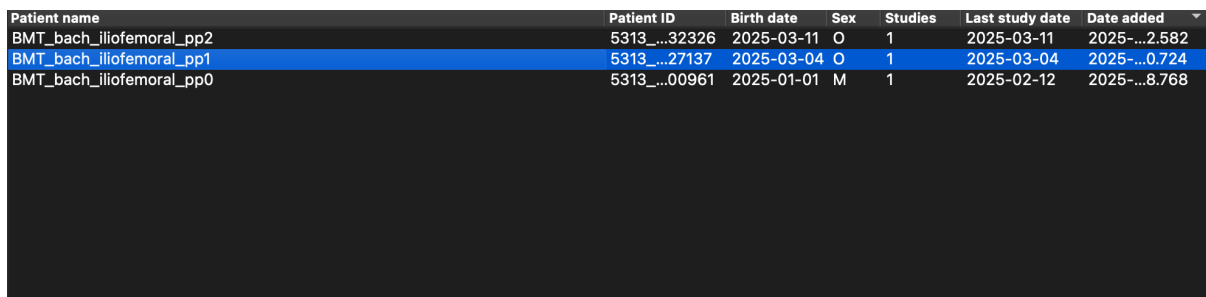
17. Select the 'Scanning Sequence' as 'SE' and the 'Sequence Name' as 'FSE REL' ;
18. Fill out the series description as '81°- FSE T2 sagittal blackblood'.;
19. Set the parameters of the sequence to the values in table 1 in section 3.1.1 and place the scanning region as in Figure 10B ;
20. Perform T2 FSE sequence with the participant in the upright position;
21. Select the 'Scanning Sequence' as 'GR' and the 'Sequence Name' as 'GE' ;
22. Fill out the series description as '81°- TOF, TE=10, HR';
23. Set the parameters of the sequence to the values in table 2 in section 3.1.2 and place the scanning region and saturation block as in Figure 12. Set 'speed up acquisition' to **off** ;
24. Perform Gradient Echo Time-of-Flight (TOF) sequence;
25. The upright scanning is now finished. Inform the participant that the MRI system will be tilted back to an angle of 0°;
26. The supine scanning can commence. Repeat steps 10, 11, 12 and 13;
27. Perform Scout sequence;
28. Repeat step 17;
29. Fill out the series description as '0°- FSE T2 sagittal blackblood' and repeat step 19;
30. Perform T2 FSE sequence with the participant in supine position;
31. Repeat step 21;
32. Fill out the series description as '0°- TOF, TE=10, HR' and repeat step 23;
33. Perform Gradient Echo Time-of-Flight (TOF) sequence;

34. The second part of the scanning is now finished. The MRI system can remain at a tilt angle of 0° for the last part of the scanning protocol;
35. Inform the participant that the last part of the scanning will now take place and that the legs will be tilted upward for the final part by placing a cushion under the legs. Then, place the cushion and check if the participant is still comfortable. The participant is now in the hip-flexed position;
36. Repeat steps 10, 11, 12 and 13;
37. Perform Scout sequence;
38. Repeat step 17;
39. Fill out the series description as '0°- FSE T2 sagittal blackblood'. If desired, add a notion of the hip-flexion to the series description and repeat step 19;
40. Perform T2 FSE sequence with the participant in hipflexion position;
41. Repeat step 21;
42. Fill out the series description as '0°- TOF, TE=10, HR'. Again, if desired, add a notion of the hip-flexion to the series description and repeat step 23;
43. Perform Gradient Echo Time-Of-Flight (TOF) sequence;
44. All scanning is now finished. Inform the participant of this. Remove the cable of the coil from the MRI system and finally remove the coil from the MRI table. The participant may sit up again and leave the MRI system.

B '3D Slicer' protocol for diameter measurements

Version '3D Slicer': 5.8.0

1. Make sure to have the above mentioned version (or newer) of '3D Slicer' and the toolboxes 'Add DICOM data', 'Segment Editor' and the 'Vascular Modelling Toolkit' installed. The 'Vascular Modelling Toolkit' needs to be installed separately from the 'Extensions Manager' (View ⇒ Extensions Manager);
2. You can choose any lay-out you like in the software (View ⇒ Lay-out). It is advised to choose 'Conventional' or 'Conventional Plot' for this specific protocol;
3. Check if all images are in one folder on your computer. Then, using 'Import DICOM files' from the toolbox 'Add DICOM data', upload the MRI scan of interest from your computer into the DICOM library of '3D Slicer'.
4. In the '3D Slicer' DICOM library, click on the folder of the participant of which you wish to analyse the MRI scan. See Figure 26.



Patient name	Patient ID	Birth date	Sex	Studies	Last study date	Date added
BMT_bach_iliiofemoral_pp2	5313_...32326	2025-03-11	O	1	2025-03-11	2025-...2.582
BMT_bach_iliiofemoral_pp1	5313_...27137	2025-03-04	O	1	2025-03-04	2025-...0.724
BMT_bach_iliiofemoral_pp0	5313_...00961	2025-01-01	M	1	2025-02-12	2025-...8.768

Figure 26: An overview of the DICOM library in '3D Slicer'. Clicking on the folder of interest will load the DICOM data from the MRI scan in '3D Slicer'.

5. From the 'Modules' menu, open the 'Segment Editor' toolbox. Select the MRI scan you wish to analyse in the 'Source Volume' menu.
6. Create a new segment by clicking on 'Add'. If you wish to change the colour and/or name of the segment: double click on the created segment and make the desired changes in the newly opened pop-up;
7. Click on the 'Threshold' tool from the toolbox. '3D Slicer' will automatically choose an appropriate threshold based on the selected source volume. Though, it is advised to scroll through all slices of the MRI scan in the viewer and check whether the mark-ups on the slices track the shape of the vein sufficiently. If deemed necessary, change the threshold range in the menu (see Figure 27). Minor markups in other regions of the scan may occur, this is not an issue as will be explained in step 9.

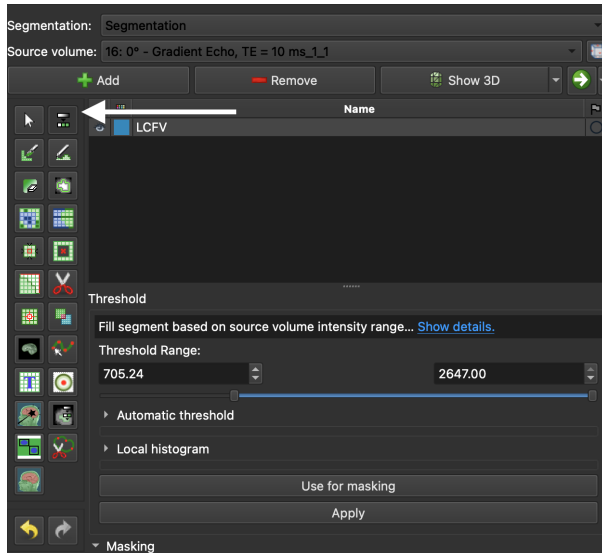


Figure 27: The threshold menu in '3D Slicer'. The white arrow points to the icon of the 'Threshold' tool from the 'Segment Editor' toolbox.

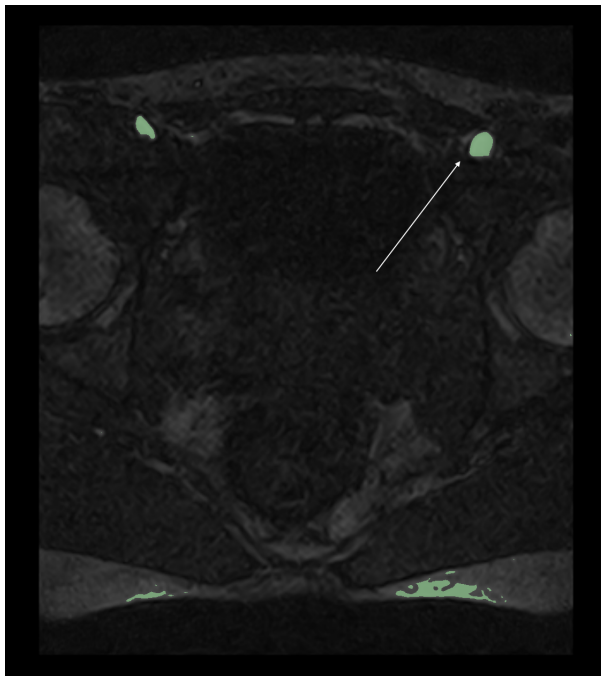


Figure 28: An example of the threshold tool markups on the acquired MRI scan. The arrow points to the markup of the region of interest on one specific slice of the MRI scan: the left common femoral vein.

8. To convert this into a three-dimensional model, click on the 'Apply' button and then on the 'Show 3D button' (See Figure 27).
9. The created three-dimensional model from the threshold markups will show in the '3D view' box. With the 'Scissors' tool in the 'Segment Editor' toolbox, remove any non-relevant structures. This includes the structures formed from the mentioned minor markups and the segment from the right common femoral vein. The model may show a venous bifurcation at the end (not always). Since it is not a part of the common femoral vein, this bifurcation should also be removed with the 'Scissors' tool.
10. '3D Slicer' automatically applies surface smoothing with a smoothing factor of 0,50. The smoothing factor can be adjusted (downward triangle next to 'Show 3D' ⇒ Smoothing factor) but it is advised to choose a smoothing factor no higher than 0,50 as a higher smoothing factor may result in specific features of the segment being removed. See Figure ?? for an example of such a three-dimensional model.

- Next, click on 'Import/export nodes' to export the created segment (see Figure 29). Check if 'Operation' is set to 'Export' and set 'Output type' to 'Models' in the newly opened menu. Finally, click on the 'Export' button (See Figure 30).

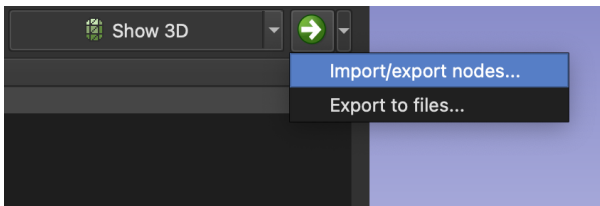


Figure 29: With this option, the created segment can be exported.

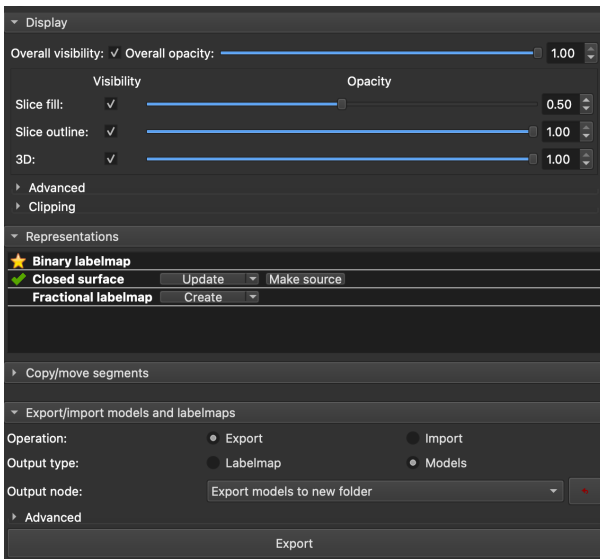


Figure 30: This menu shows the options for exportation. If it is desired, the look of the 3D model can be adjusted here as well (opacity etc).

- Using the 'Modules' menu, open the 'Extract centerline' toolbox from the previously installed 'Vascular Modeling toolkit'. Select the just exported segment under 'Inputs' ⇒ Surface (See Figure 31).
- Click on the 'Auto-detect' button, after which '3D Slicer' will detect the endpoints of the model and set a green seed at the start of the segment and a red seed at the end of the segment. The seeds can be repositioned manually if necessary. They should be placed in the middle of the top and bottom cross-section as the centreline will be drawn between these points (See Figure 31).
- Once the seeds are placed correctly, select the segment under 'Tree' ⇒ 'Centerline model' and give the centreline curve an appropriate name under 'Tree' ⇒ 'Centerline curve' (See Figure 31). Finally, click 'Apply'. The obtained centreline curve will show in the model (See Figure 32).

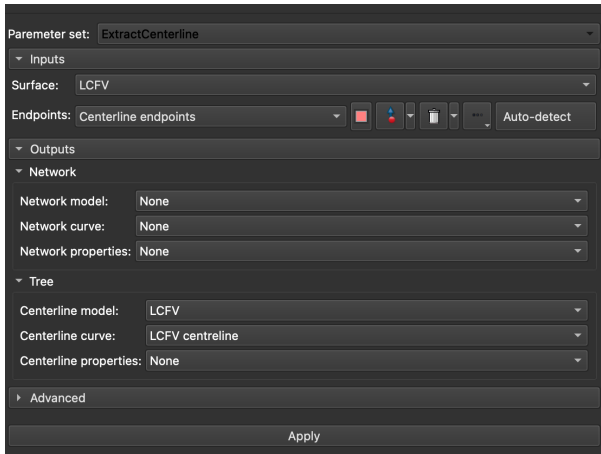


Figure 31: This menu shows the options for exportation. If it is desired, the look of the 3D model can be adjusted here as well (opacity etc).

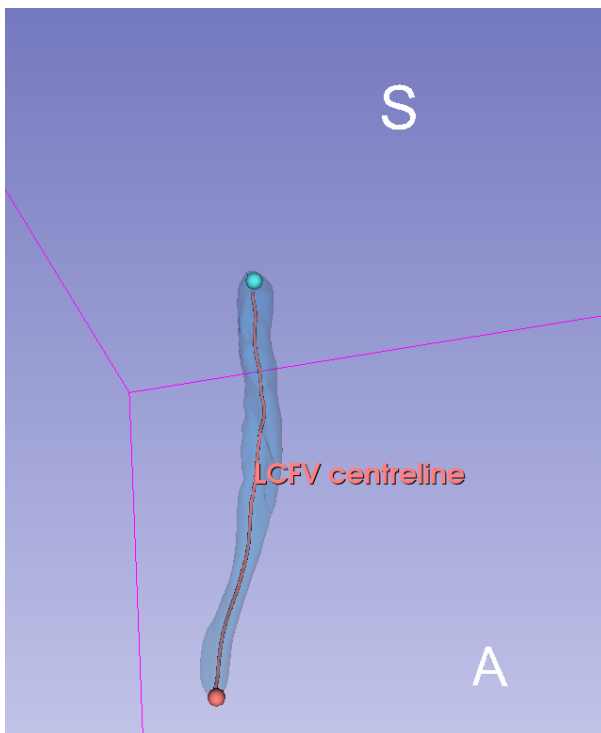


Figure 32: The 3D model with the obtained centreline curve. For the purpose of showing the centreline curve drawn into the model, the opacity of the model was set to a low value.

15. Now, go to the 'Cross-section analysis' toolbox from the 'Vascular Modeling toolkit'. In this toolbox, the diameter calculations based on the acquired three-dimensional model and the centreline can be done. '3D Slicer' offers the option of calculating and plotting either the CE diameter or the MIS diameter. Choose the acquired centreline curve as the 'Centerline source', select 'Segmentation' in the dropdown menu under 'Input lumen surface' and choose the name of the exported model under 'Segment'. Set a name for the output table and plot label under 'Output table' and 'Output plot series'. Choose the measure that is desired for the diameter analysis in the second dropdown menu of 'Output plot series'. The coordinate system was in this case set to 'RAS (Slicer convention)' for comparison with the MRI images in the red, green and yellow viewer that use the Slicer convention as a coordinate system. But, if desired, the coordinate system can also be set to 'LPS (DICOM convention)'. See Figure 33.

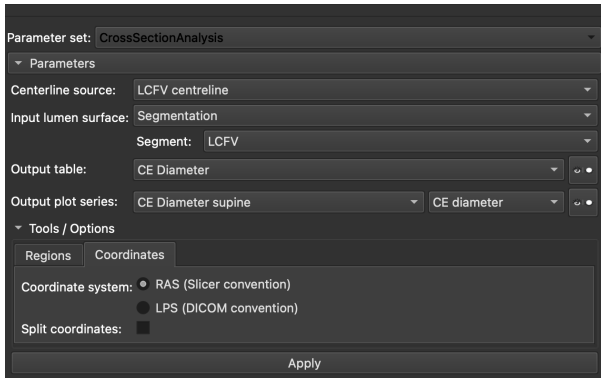


Figure 33: An overview of the settings for the diameter analysis in '3D Slicer'. Next to the 'CE Diameter', the 'MIS Diameter' is also an option.

- Run the algorithm by clicking on 'Apply'. This outputs a table and a plot of the selected diameter measure. See Figure 34.

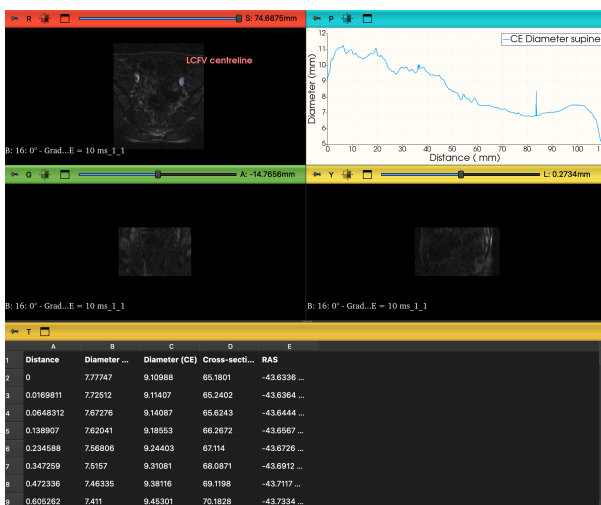


Figure 34: '3D Slicer' can show a plot and a table of the calculated diameters in the selected measure.

- '3D Slicer' can show some statistics on the diameter analysis. Namely, the minimum and maximum MIS diameter in the segment, its corresponding CE diameter, its coordinates and its location on the centreline (measured from the origin of the centreline). The same statistics are available for the minimum and maximum cross-section area of the segment and by moving the 'Point Index' bar, for all points on the centreline. See Figure 35.

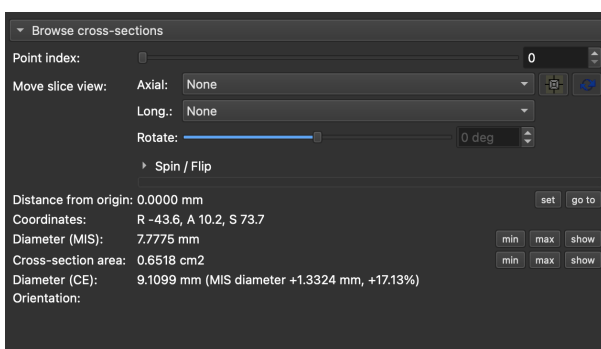


Figure 35: '3D Slicer' can show statistics of diameter measurements and cross-section area along each point on the centerline of the segment.

- The MIS diameter and cross-section area of the segment can be viewed along each point on the centreline of the model by clicking on the 'Show' button (Figure 35). See Figures 36 and 37 for an example of this.

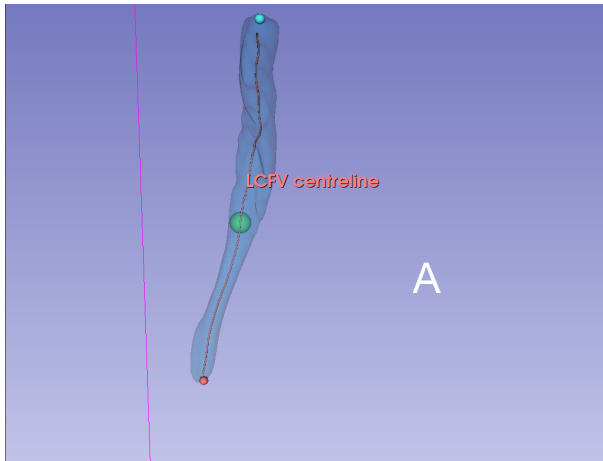


Figure 36: The maximum inscribable sphere at an arbitrary point along the centreline. Also known as the 'MIS diameter'.

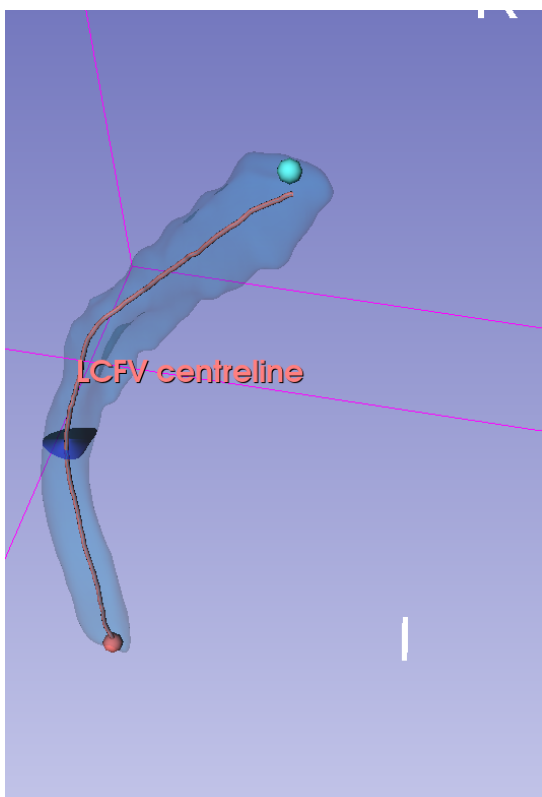


Figure 37: With '3D Slicer', the cross-section area along each point on the centerline can be calculated and shown within the model of the segment.

19. If desired, the values of the output table can be exported to a file in the 'Data' module. In the 'Subject hierarchy' overview in this module, click on the name of the table that is shown, in the pop-up menu choose 'Export to file...' upon which it can be chosen to export it to .tsv, .csv or .txt file. With the exported file, further analysis in, for example, Python or MATLAB is possible.